

19

A NEXT-GENERATION MICROWAVE RAINFALL RETRIEVAL ALGORITHM FOR USE BY TRMM AND GPM

Christian Kummerow¹, Hirohiko Masunaga¹, and Peter Bauer²

¹*Department of Atmospheric Science, Colorado State University, Fort Collins, CO, USA*

²*European Centre for Medium-Range Weather Forecasts, Reading, UK*

1 INTRODUCTION

Passive microwave rainfall algorithms have evolved steadily from those designed for the early Electronically Scanning Microwave Radiometer (ESMR), through the Scanning Multichannel Microwave Radiometer (SMMR) on Nimbus-7, and the Special Sensor Microwave Imager (SSM/I) instruments flying on the Defense Meteorological Satellite Program (DMSP). A number of algorithms fitting roughly three classes have emerged. These are (a) the “emission type” algorithms (e.g., Wilheit et al. 1991; Berg and Chase 1992; Chang et al. 1999) that use low-frequency channels to detect the increased radiances due to rain over radiometrically cold oceans; (b) the “scattering” algorithms (Spencer et al. 1983; Grody 1991; Ferraro and Marks 1995) that correlate rainfall to radiance depressions caused by ice scattering present in many precipitating clouds; and (c) the “multichannel inversion” type algorithms (Olson 1989; Mugnai et al. 1993; Kummerow and Giglio 1994; Smith et al. 1994; Petty 1994; Bauer et al. 2001; Kummerow et al. 2001) that seek to invert the entire radiance vector simultaneously. Among these, the Wilheit et al. (1991) and Kummerow et al. (2001) algorithms are used operationally for the Tropical Rainfall Measuring Mission (TRMM) Microwave Imager (TMI) as well as the Advanced Microwave Scanning Radiometer (AMSR-E) flying on Aqua, while the Wilheit et al. (1991) and Ferraro and Marks (1995) algorithms are used with SSM/I in the Global Precipitation Climatology Project (GPCP) over ocean and land, respectively. The Bauer et al. (2001) algorithm is used at ECMWF

for rain assimilation experiments. In each case, algorithms have been optimized for the corresponding satellite sensor.

Algorithm intercomparison efforts, initially aimed at identifying the “best” algorithms have not been able to make much headway, as each algorithm appears to have strengths and weaknesses related to specific applications, while none appears to be universally better than the others.

The next advance in global precipitation monitoring, the Global Precipitation Measurement (GPM) mission, is providing new impetus towards a common algorithm framework. The GPM concept consists of a core satellite, with a dual-frequency precipitation radar (DPR), and a multichannel microwave imager (GMI). This component is similar in concept to the TRMM design but with improved radar capabilities and an orbit that will cover between 65–70° of latitude. In addition, the GPM concept uses a constellation of operational and dedicated radiometers to produce global, three hourly rainfall products required by many applications. The fact that radiometers for the GPM constellation are not fully specified and will evolve throughout the mission based on contributions from a number of different space agencies immediately imposes a number of high-level requirements upon any algorithm designed for these sensors.

Of utmost importance is the need for a transparent, parametric algorithm that insures uniform rainfall products across all sensors. The requirement for transparency is clear. A mission of GPM’s scope should not rely on a single black box operated by any one individual. Instead, it requires an open architecture that will allow the international community to participate in the algorithm development, its refinement, and its error characterization. The requirement for a parametric algorithm is also self-evident. Since GPM is being designed as an ongoing cooperative concept among many agencies, algorithms cannot be designed for specific radiometers with defined frequencies, viewing geometry, spatial resolutions or noise characteristics. The algorithm should be applicable to any sensor. Such a requirement leads naturally to a generalized framework that avoids the need for specific frequencies for their application. Finally, the algorithm should be robust in such a way that differences between sensors can be confidently interpreted as physical differences between observed scenes rather than artefacts of the algorithm.

Together with the above requirements, algorithms designed for the future should also be able to fully characterize uncertainties at any space and time scale being considered by the users. This ranges from instantaneous estimates needed for many hydrologic and weather forecasting applications to large space and time averages required for climate model verification and climate trend monitoring. While such a requirement is also perhaps self-evident, such a complete error characterization does not currently exist and is undoubtedly the greatest challenge facing the community.

2 THE ALGORITHM

Rainfall retrieval algorithms are not fully constrained. Instead, *a priori* information must be supplied to help constrain the estimated 3-dimensional (3D) properties of precipitating clouds. The requirement that the GPM algorithm be adaptable to any satellite sensor and that it produces realistic uncertainty estimates for global application reduces the large set of previous algorithms to those that involve physical forward/inverse modeling where the statistical properties of the *a priori* information and the models can be formulated in a consistent way. In a physical framework, the optimum estimate of a state vector (precipitation profile), \mathbf{x} , must be obtained using an observation vector (brightness temperatures), \mathbf{y} , plus additional *a priori* information.

Due to errors in modeling and observation (error covariance \mathbf{R}), the relation between state and observation is usually described by probability density functions (pdf's). This can be formalized with Bayes' theorem (e.g., Rodgers 2000):

$$P(\mathbf{x} | \mathbf{y}) = \frac{P(\mathbf{y} | \mathbf{x})P(\mathbf{x})}{P(\mathbf{y})} \quad (1)$$

$P(\mathbf{x}|\mathbf{y})$ is the *posteriori* probability of \mathbf{x} when \mathbf{y} is observed. $P(\mathbf{y}|\mathbf{x})$ is the probability of making observation \mathbf{y} when \mathbf{x} is present, while $P(\mathbf{x})$ and $P(\mathbf{y})$ are the *a priori* probabilities of \mathbf{x} and \mathbf{y} , respectively. The latter may come from global statistics of state and observations. The determination of $P(\mathbf{y}|\mathbf{x})$ requires a model that translates between state and observation space. This model may also be used to compute $P(\mathbf{y})$ if $P(\mathbf{x})$ is assumed to fully describe the *a priori* distribution of \mathbf{x} . Examples of the application of the above principle are the 'Bayesian' rainfall retrieval schemes that found rather wide distribution in recent years (Evans et al. 1995; Kummerow et al. 1996; Olson et al. 1996; Haddad et al. 1997; Marzano et al. 1999; Bauer et al. 2001, Kummerow et al. 2001; Viltard et al. 2004).

One particular problem associated with these rainfall retrievals is that the model that connects states and observations, i.e., $\mathbf{y} = \mathbf{F}(\mathbf{x}) + \boldsymbol{\epsilon}$ (where $\boldsymbol{\epsilon}$ is the modeling error), is generally nonlinear. This immediately implies that the inversion of this relation is state dependent, and the inversion must be formulated differently depending on whether (a) a first guess of the actual state, \mathbf{x}_b , and its error covariance, \mathbf{B} , is known and Gaussian with respect to the true state or (b) only a pdf of state \mathbf{x} is known from which the pdf of \mathbf{y} can be calculated. If (a) applies, Eq. (1) can be transformed to:

$$P(\mathbf{x} | \mathbf{y}) = \exp\left\{-\frac{1}{2}[\mathbf{y} - \mathbf{F}(\mathbf{x})]^T \mathbf{R}^{-1}[\mathbf{y} - \mathbf{F}(\mathbf{x})] - \frac{1}{2}[\mathbf{x} - \mathbf{x}_b]^T \mathbf{B}^{-1}[\mathbf{x} - \mathbf{x}_b]\right\} \quad (2)$$

The probability of $P(\mathbf{x}|\mathbf{y})$ is maximized when the first derivative of Eq. (2) vanishes. This can be solved numerically by iterative procedures, and represents the “variational” retrievals. If Eq. (2) applies, it is more appropriate to seek the expected value of \mathbf{x} . From practical considerations, the expected value is often expressed as (Olson et al. 1996):

$$E(\mathbf{x}) = \frac{\sum_i \mathbf{x}_i \exp\{-0.5[\mathbf{y} - \mathbf{F}(\mathbf{x}_i)]^T \mathbf{R}^{-1}[\mathbf{y} - \mathbf{F}(\mathbf{x}_i)]\}}{\sum_i \exp\{-0.5[\mathbf{y} - \mathbf{F}(\mathbf{x}_i)]^T \mathbf{R}^{-1}[\mathbf{y} - \mathbf{F}(\mathbf{x}_i)]\}} \quad (3)$$

even though the formulation in Eq. (3) makes the assumption that $P(\mathbf{x})$ and $P(\mathbf{y})$ are well known. This will be called “Bayesian” method even though both approaches are based on Bayes’ theorem.

Both solutions employ a forward model that often consists of combined cloud resolving and radiative transfer models, the latter involving clear-sky atmospheric and surface models. In the variational framework, these models have to be directly inverted because the difference between model-calculated and observed brightness temperatures must be translated into increments to the initial physical state. Here, adjoint models have recently been developed for rainfall retrieval purposes (Moreau et al. 2003). The first-guess state and its error characteristics, however, are difficult to obtain for precipitation and this method is only possible in a well-constrained large-scale model (Moreau et al. 2003, 2004). The main advantage of such a method is its global applicability and its flexibility with respect to any input data, while its disadvantage is the requirement of a well-defined first guess and the computational cost. In the Bayesian method, the biggest challenge is the definition of the *a priori* database, $P(\mathbf{x})$, because it is not well known for precipitating clouds. Historically, Bayesian schemes used precipitation profiles derived from a set of existing cloud-resolving model (CRM) simulations to construct the *a priori* database of potential precipitation structures that might be seen by a radiometer. The CRMs provide a physically consistent set of full 3D hydrometeor and latent heating profiles. They also provide a simple method to use understood physical processes to constrain an inversion. The biggest disadvantage of the Bayesian algorithm is its lack of general applicability because only a few CRM simulations are available (and useful) to construct a valid $P(\mathbf{x})$. A first-guess constraint may be possible to help constrain $P(\mathbf{x})$ in the future. Inherent to both methods is the impact of the dynamical and microphysical formulations in the forward model that often dominate the uncertainties of the radiative transfer modeling.

3 THE PARAMETRIC ALGORITHM FRAMEWORK

Most likely, future algorithms will be composed of elements present in both approaches, i.e., pdf-type estimators with static databases and variational elements where reliable first-guess information is available. The Bayesian, as well as variational techniques have the added advantage that they are intrinsically parametric and uncertainties in the *a posteriori* rainfall can be computed in a straightforward fashion. Nonetheless, the approaches are not without pitfalls. Variational approaches are contingent upon a good first guess, which is often difficult to make in the case of precipitation systems. Current Bayesian schemes, in addition to relying on incomplete CRM simulations, use procedures such as rainfall screening, freezing-level estimates and convective/stratiform classification in order to improve the retrieval performance. Incomplete databases require procedures to solve the problem when none of the simulated profiles are close to the observed brightness temperature vector.

More subtle, but perhaps more important to both schemes, are the errors in the *a priori* database itself. Errors in the CRM simulations will cause radiometers with different channel combinations to retrieve different rainfall amounts. This potential aliasing is simple to illustrate with a hypothetical CRM that consistently produces too much ice in the simulation—thus creating simulations with large Tb depressions at high frequency for even modest rainfall rates. A sensor with only low frequency channels (e.g., 10–37 GHz) may not be susceptible to this problem and will retrieve approximately the correct rainfall (all else being correct). A sensor with only high frequency channels (e.g., 85 and 150 GHz), on the other hand, will match large Tb depressions to relatively modest rain cases with large Tb depressions found in the CRM simulation. This will cause a consistent underestimation and a different result than that obtained from the first sensor.

Conceptually, a parametric algorithm must therefore address two distinct issues. It must avoid any channel specific procedures in the algorithm, and it must create an *a priori* database that is consistent with all the brightness temperatures that may be observed by individual radiometers. Avoiding channel specific procedures will be seen to be a relatively straightforward task in both the Bayesian and variational frameworks. Building a representative *a priori* database with a verifiable error model is a far more challenging task. The error model, in particular, is very difficult to construct because of the role of CRMs in the forward computations. While they are useful in the sense that they add physical constraints to the clouds that may be retrieved, they are extremely difficult to verify quantitatively since they are constructed to simulate physically consistent scenes rather than the details

of any one observed cloud realization. A more complete and verifiable *a priori* database appears thus to be crucial for any algorithm in the GPM era.

Following is a description of a prototype parametric algorithm using both variational as well as Bayesian methods. While the various aspects of the algorithm are being developed separately and for different sensors, they are presented here as parts of the same conceptual algorithm for illustration purposes. In this conceptual algorithm, the *a priori* database is constructed from a combination of TRMM precipitation radar (PR), TMI and CRM information when the TMI footprint contains rainfall as determined from the PR. When the radiometer footprint does not contain rainfall, a variational technique is used with the radiometer data to obtain the clear air parameters. Together, these two components lead to a consistent 3D distribution of geophysical parameters that are fully representative of the observed scenes and fully consistent with the observation vector. Benefits of this more representative database are discussed in Viltard et al. (2004). The rainfall retrieval itself follows the Bayesian formalisms cited earlier.

3.1 The non-raining simulations

Over oceans, passive microwave radiances depend upon column-integrated water vapor, cloud liquid water, sea surface temperature, and surface wind speed. These geophysical parameters can be retrieved simultaneously from the TMI itself for which the TRMM PR shows no rainfall. Techniques such as those described in the literature (e.g., Wentz 1997) do exactly this. Unfortunately, that technique has some shortcomings with respect to the current objectives. It only works over ocean, and it seeks consistency only among the channels used in the particular inversion.

An alternative algorithm for clear-sky applications makes use of the previously introduced variational approach. Due to the many free parameters, in particular over land surfaces, the physical framework has to be kept very simple and only a few bulk parameters may be retrieved. As an example, we chose a set of four or six free parameters for ocean and land, respectively. Over ocean, these are surface skin temperature, near-surface wind speed, water vapor path, and cloud liquid water path, while over land these are surface skin temperature, effective water coverage, vegetation coverage, surface roughness, water vapor path, and cloud liquid water path. The surface skin temperature also determines the effective atmospheric temperature by assuming a constant lapse rate. The effective atmospheric temperature has to be understood as the temperature of the lower atmosphere where most of the water vapor is present, while the effective water coverage over land summarizes the true coverage with open water and soil moisture. The effect of soil moisture and open water on land surface emissivity is very similar. Atmospheric absorption was calculated according to Liebe et al. (1992), sea-surface emissivity with the model of Ellison et al.

(2003) and land surface emissivity with the model of Bauer and Grody (1995). The atmosphere consists of seven layers with constant depths.

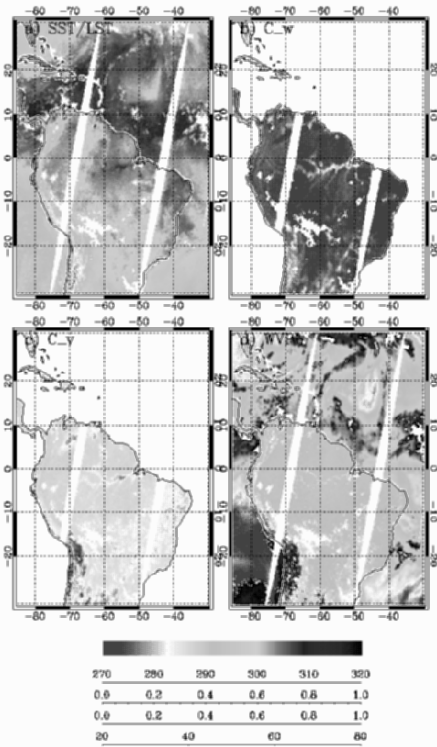


Figure 1. Example of variational retrieval of surface skin temperature (a), effective water coverage (b), effective vegetation coverage (c) and water vapor path (d) using SSM/I data on November 1, 2003. Scales at the bottom refer to units [K], [], [], [kg m⁻²], respectively.

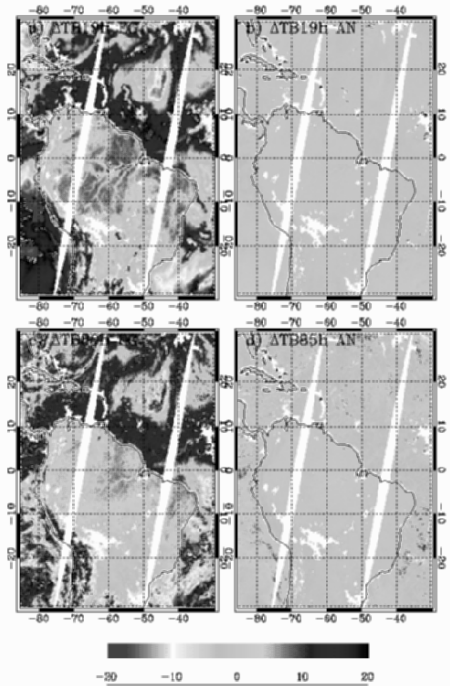


Figure 2. TB-departures (observation minus simulation) using first-guess (a, b) and after variational retrieval (c, d) at 19.35 GHz (a, c) and 85.5 GHz (b, d) and horizontal polarization. Scales at the bottom refer to units [K].

First-order climatological values were assumed for the above parameters to initialize the minimization of some SSM/I overpasses over South America and the Southern Caribbean on November 1, 2003. Figure 1 shows the resulting retrievals for the surface skin temperature, effective water coverage, vegetation coverage and water vapor path, respectively. The fields represent reasonable distributions showing the Amazon River basin in both Fig. 1b and 1c as well as the orography-dependent surface temperature distribution. The water vapor fields over ocean reach very low values in the presence of clouds, which indicate a possible aliasing effect between water vapor and liquid water absorption. Nonetheless, these results indicate that a variational retrieval is feasible for clear-sky applications providing background fields

for the hydrometeor retrievals in the presence of rain. More realistic first-guess values as well as error covariances may be obtained from climatological fields produced by global model analyses. Potential refinements in the physical models used in the inversion may also lead to further improvements.

Figure 2 illustrates the brightness temperature departures before and after the retrieval at 19.35 and 85.5 GHz. The departures are quite large in areas with strong water vapor gradients and in the presence of clouds over sea with values above 20 K. This indicates that the first-guess values chosen for this example are only appropriate for illustration rather than operational application; however, the minimization performs well and reduces the departures to within instrument error limits. Clouds and light precipitation may be present in those areas where large departures remain after the retrieval (in particular at 85.5 GHz). The problem with precipitation is artificial, as the real database would be constructed from TMI data for which rain/no rain information is available from the PR.

3.2 The raining scene

Figure 3 illustrates the overall flow of the algorithm described here to derive precipitation profiles consistent with both radar and radiometer measurements. The non-raining parameter retrievals, indicated by blue-colored items in Fig. 4, were introduced in the previous section. In this section, the rain-profiling scheme using PR, TMI, and CRM information is outlined.

The PR identifies pixels with radar echoes significantly above the noise threshold as “rain certain.” The weakest detectable signal by PR corresponds roughly to 0.5 mm h^{-1} in rain rate. The GPM 35-GHz radar is currently planned to have a threshold of approximately 12 dBZ, which corresponds to roughly 0.2 mm h^{-1} . If PR detects a rain signal, the rain profile that best fits the PR reflectivity profile is selected from a set of precomputed CRM simulations. The reflectivity of the cloud-model profiles was obtained by computing single particle backscattering and extinction properties based upon Mie theory and assuming a gamma drop size distribution (DSD) with a given median volume diameter (D_0) and $\mu = 3$.

As an example, the initially assumed DSD model may be taken, which was constructed to be consistent with the Z-R relations assumed in the TRMM PR operational rain-profiling algorithm (2A25) developed by Iguchi et al. (2000). The particle size distributions of other hydrometeor species are the same as adopted by the CRM except for melting particles. Here, the microwave properties of melting hydrometeors are simplified in such a way that the particle size distributions are linearly transformed under an averaged dielectric function from ice to liquid within a half-kilometer layer below the freezing height. This simplified treatment of melting particles could be

replaced with a more elaborate microphysical model in the future (Bauer 2001; Olson et al. 2001; Battaglia et al. 2003).

The CRMs used in the study were the Goddard Cumulus Ensemble Model (GCE) and the University of Wisconsin Non-hydrostatic Modeling System (UW-NMS), which are the same simulations used in the *a priori* database used in the Goddard Profiling Algorithm (Kummerow et al. 2001).

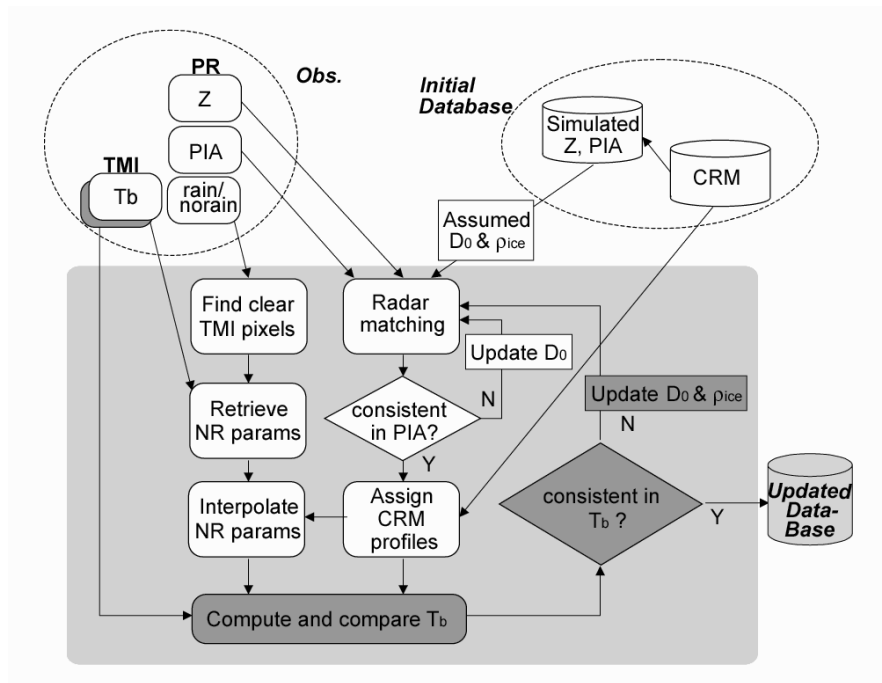


Figure 3. Algorithm flowchart. Blue colored items are related to the non-raining (NR) parameter retrieval, yellow to the PR profile matching, and red to the comparison of matched profiles in the Tb space.

The best fit in the PR reflectivity matching is defined as the one having the least root-mean-squared difference between observed (PR-1C21 attenuation-uncorrected reflectivity) and computed reflectivity. When the observed Path-Integrated Attenuation (PIA) from the PR is sufficient to provide a robust signal, there is additional DSD information available from the radar. In this case, the best-fit solution with respect to both the reflectivity profile as well as the PIA is sought by searching simulated profiles with several different DSD assumptions.

While computationally different from the PR algorithm developed by Iguchi et al. (2000), philosophically this step matches the PR procedure by

adjusting the retrieved DSD to match both the reflectivity and the PIA when it is deemed robust. Figure 4 shows a snapshot of surface rain rate given by the matched CRM profile and 2A25 surface rain, exhibiting good qualitative agreement. A direct pixel comparison of the observed and reconstructed

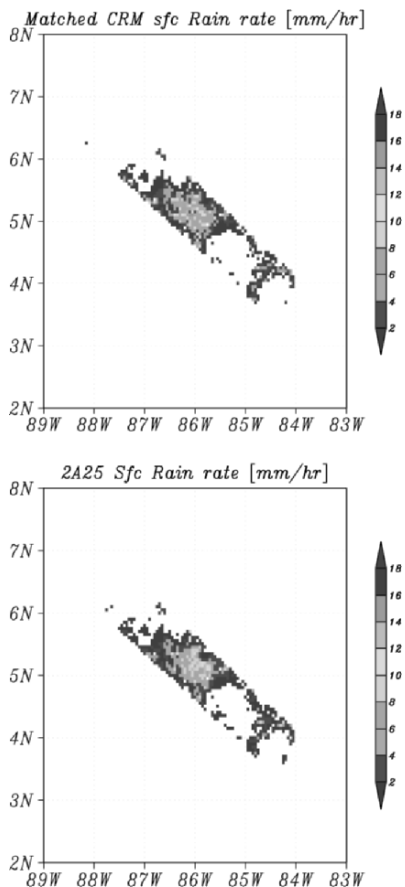


Figure 4. Top: Surface rain rate given by CRM profiles that best fit the measured PR profiles. Bottom: 2A25 surface rain rate for the same scene as the top panel.

surface rainfall for this scene shows a bias of 1.5% with a correlation of 0.96. The light grey portion of Fig. 3, which includes an iterative step if PIA is robust, shows the flow of the above procedure.

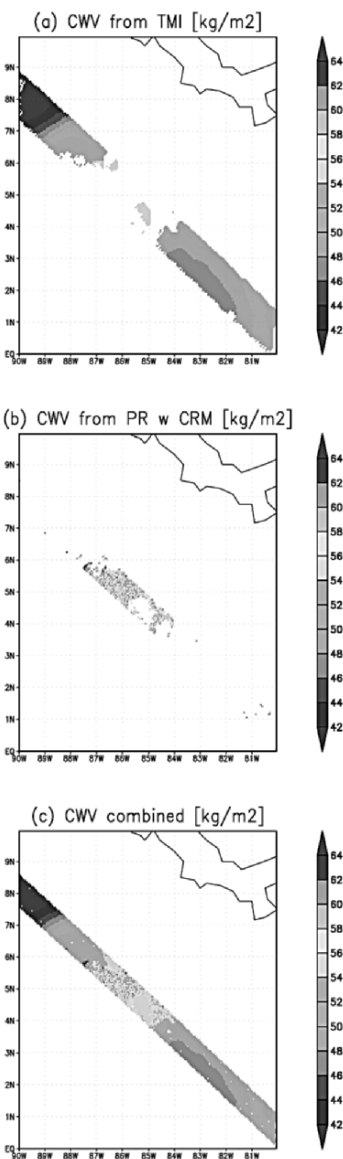
At this point in the retrieval, the raining and non-raining scenes must be merged. As discussed in the previous section, the non-raining retrievals are applied to all TMI footprints in which PR observed no rain. The rain retrieval, however, is applied to PR pixels that generally have higher spatial resolution than the TMI footprints. This difference in resolution can lead to small areas within partially raining TMI footprints for which the clear air retrieval could not be performed but for which PR observes no rain.

These areas must be filled by an interpolation scheme before the final step in the raining retrieval can be completed. This interpolation scheme is also used to prescribe the surface conditions under the raining pixels.

Figure 5 illustrates this procedure, originally developed by Shin and Kummerow (2003), for the cloud liquid water field over ocean. All clear air fields are treated in a similar manner. Figure 5a represents the TMI retrieval for column water vapor (CWV) in this example. Figure 5b shows the CWV field associated with the raining retrievals, and Fig. 5c the final CWV field in which TMI CWV has been mapped to PR pixel locations and missing values have been interpolated. The slightly lower CWV values in precipitation (relative to the non-raining surroundings) might be an artifact

of the algorithm still under development. Inspection of the raining profiles, however, indicate they are nearly all saturated. As such, the lower CWV values might be real if one takes into account the lower temperatures associated with evaporation cooling associated with light precipitation. The interpolation over land will introduce greater uncertainties as the effective water coverage, vegetation cover, and surface roughness can vary rapidly.

Precipitation profiles obtained from the PR matching technique are assigned to the satellite swath. The geophysical parameters unobservable by PR such as SST, surface wind speed, water vapor, and cloud water are provided from the TMI retrieval in non-raining scenes and interpolated to the



raining field of view (FOV). Radiative transfer calculations using the Eddington approximation (Kummerow 1993) are then performed along slant paths that intersect a few neighboring PR pixels to properly take into account the TMI incidence angle of 52.8°. The computed brightness temperatures are convolved with the Gaussian antenna pattern using the 3-dB-beam width of each TMI channel. Figure 6 shows the retrieved liquid and ice water contents, along with the computed brightness temperatures along the scan center of the rain feature shown in Fig. 4. The observed and computed brightness temperatures generally exhibit good but not perfect agreement.

Figure 5. Simulation steps for a non-raining scene over ocean. (a) Shows the columnar water vapor retrieved from the TMI data for pixels in which PR detected no rain. (b) Column water vapor in raining pixels as determined through the selected cloud resolving model profile. (c) The merged and interpolated final column water vapor field.

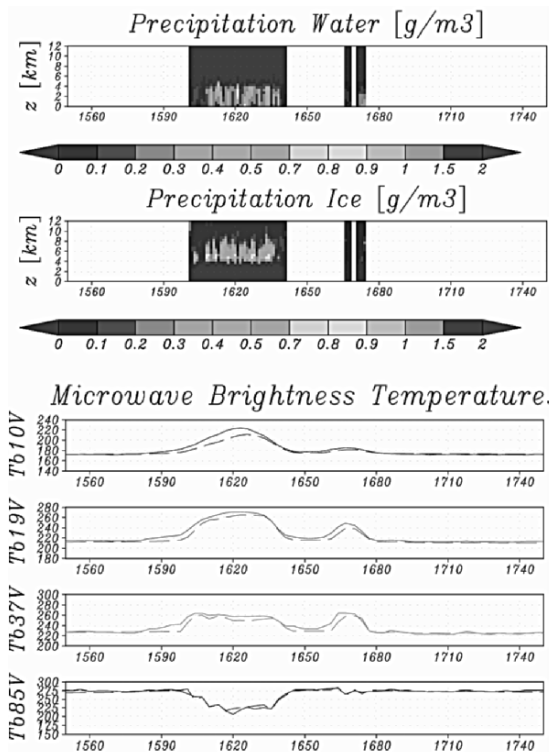
The dark grey portion of Fig. 3 summarizes the final procedure. If the computed Tb's at the lower frequency channels are lower than the observed ones, the assumed drop sizes can be decreased in order to increase the liquid water content determined from PR. As can be seen from the diagram, however, this can only be done for those pixels for which PR is not able to determine its own DSD through the PIA estimate. Variational

methods that seek to adjust the DSD to simultaneously fit PR and TMI observations are also possible. Such solutions may eventually prove superior to the current approach. They are, however, less transparent.

In the current formulation, the final iterative procedure will adjust DSD, but only if the DSD is the one assumed by PR and not when it can be directly observed by the sensor. In addition to any Tb disagreements in the emission channels, Fig. 6 shows occasional discrepancies in the scattering channel (85 GHz), which can be attributed to an uncertainty in the microphysical treatment of ice hydrometeors in CRM. This discrepancy is minimized by interactively updating the ice density in the CRM model. Precipitation profiles consistent with both radar and radiometer are thus obtained by repeating the entire procedure with updated DSD and ice density models.

3.3 The *a priori* databases

Construction of the *a priori* databases is straightforward once the 3D raining and non-raining parameters derived from TRMM TMI and PR swath overlap



data have been determined. Compared to previous efforts that relied solely on the CRMs to provide cloud structures, the current methodology insures that the *a priori* database is more fully grounded in observations, which would improve the databases' representativeness of actual rainfall spectra.

Figure 6. Top two panels: Vertical cross section at the scan center of precipitation water and ice given by CRM profiles that best fit the measured PR profiles. Bottom four panels: Observed TMI brightness temperatures (solid lines) and computed brightness temperatures (dashed lines) at 10 GHz, 19 GHz, 37 GHz, and 85 GHz (vertical polarization).

Through the database construction process, furthermore, it is possible to relate the derived rainfall profiles to the environmental geophysical parameters controlling rainfall formation such as surface and upper-level

humidity, wind velocity field, freezing height, and aerosols using other satellite retrievals and/or objective analysis data archives. Since a set of observed brightness temperatures are not always sufficient to single out a proper rainfall profile, those quantities could be used to separate and index the databases to better constrain the retrieval. The resultant *a priori* databases would not only improve the algorithm performance but also provide climatological insights on the physical processes governing rainfall properties.

A priori databases can be constructed for any sensor once the sensor characteristics are defined. One important exception is that the current procedure only refers to microwave window channels. Sounding channels in the 60- and 118-GHz oxygen absorption bands as well as the 183-GHz water vapor absorption channels depend upon details of the temperature or humidity profiles that are not observed directly by TRMM. These are not well represented by the above procedure and would not be well represented by the *a priori* database.

3.4 The retrieval

Once the *a priori* databases of hydrometeor profiles and clear scenes, as well as their corresponding T_b 's are constructed for each sensor, a Bayesian retrieval methodology can be used to select those profiles that are consistent with the observations.

Synthetic retrievals using procedures similar to those described here for a number of radiometer designs are presented in Shin and Kummerow (2003). Synthetic, in this case, meant that satellite brightness temperatures were simulated from the 3D geophysical parameter derived for the *a priori* database.

Results from that work shows very small biases between satellites (<2%) and root mean square retrieval errors that varied with satellite instrument specifications, as one would expect. Radiometers with higher spatial resolutions and more channels tended to outperform less sophisticated sensors. The most important radiometer characteristics needed to reduce random errors appear to be the availability of low frequency channels (sensitive to liquid water emission) with good spatial resolution.

Results from a simplified implementation of the algorithm described here are shown in Fig. 7. The simplified scheme uses only the brightness temperature difference ($T_{b_V} - T_{b_H}$) at 19 GHz in the retrieval. This use of 19-GHz channels is not necessarily a simplification as a sensor may well exist that only has these channels.

The simplification was introduced by directly using the TRMM PR rainfall product plus some arbitrary but constant assumptions to compute T_b s needed in the *a priori* database. An additional simplification was made to use observed rather than computed brightness temperatures for the rain-free

scenes. This is equivalent to the procedure described earlier, but only applicable to the TMI instrument as the observed Tb cannot be readily transformed to other sensors. The simple algorithm is used primarily to analyze error characteristics of the more complex retrieval algorithms. As such, it is functionally quite similar to the main algorithm presented here but not parametric.

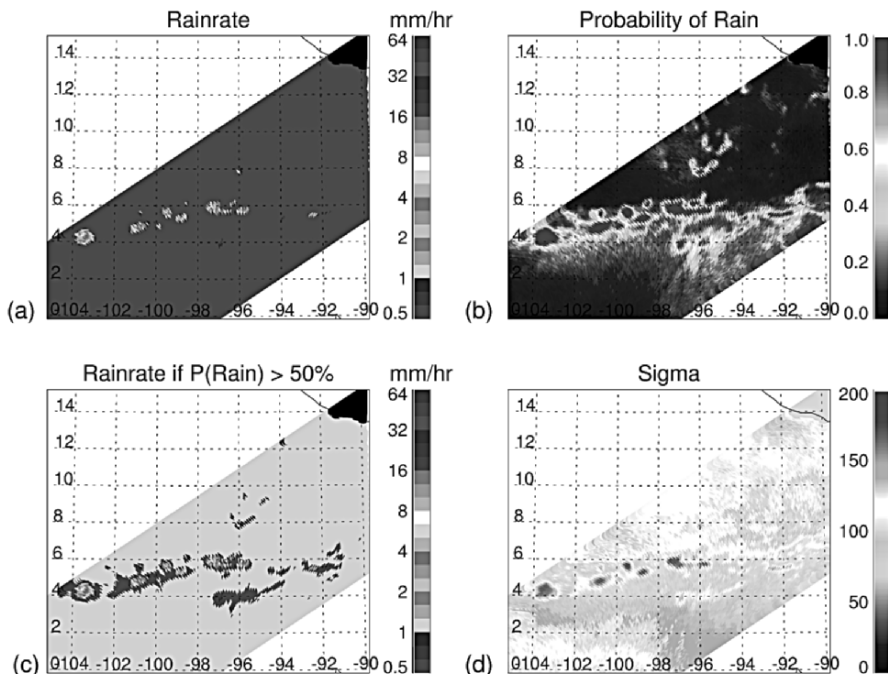


Figure 7. (a) Retrieved conditional rainfall. (b) The probability of rain. (c) Retrieved conditional rain for probability of rain greater than 50%. (d) Uncertainty of rain [%] (see also color plate 6).

Panel (a) of Fig. 7 shows the retrieved rainfall rate. The entire area is covered by light rain surrounding smaller convective cores. The 100% rain coverage may seem physically unreasonable. What is shown, however, is the conditional rain rate. Panel (b) shows the probability of rain as derived from a lookup table correlating the observed Tb and sea surface temperature to the probability that PR saw rain in that radiometer FOV. The area of light rain can be seen to have a fairly low but nonzero probability of rain and as such may still seem unphysical. The plot is shown to illustrate the probabilistic nature of the Bayesian schemes described here. Because the radar observes small, but nonzero rain probabilities for virtually all observed 19-GHz Tbs,

the retrieval cannot arbitrarily use a T_b threshold for a rain/no rain discrimination without introducing errors. Panel (c) shows the same results as panel (a), but with about 50% probability of rain threshold. This may be a more conventional approach to showing rain maps. Panel (d) provides the instantaneous uncertainty (expressed in %) of the retrieved rainfall. Areas of light rain have large percentage errors, while moderate rain has significantly more signal. These results match Viltard et al. (2004) who found similar numbers with a different implementation of a Bayesian approach.

4 THE ERROR MODEL

There are many sources of error that must be carefully defined if true uncertainties are to be quantified. Both Bayesian and variational retrievals principally imply an error calculation (Olson et al. 1996; Kummerow et al. 1996; Marzano and Bauer 2001; Bauer et al. 2002). Yet, the intrinsic uncertainties computed from these schemes are only one component. The Bayesian scheme has four independent sources of error. These are (1) the uncertainties introduced by imperfect or incomplete data used to construct the *a priori* database; (2) the uncertainty introduced by the inversion methodology; (3) the uncertainty resulting from potentially unknown changes in regional and seasonal cloud properties; and (4) the uncertainty introduced by any errors in the algorithm formulation. The Bayesian methodology deals only with the second source of error. The variational approach is less susceptible to database errors, particularly if the first-guess field is robust. Variational approach uncertainties, however, can be computed explicitly only for linear inversions. As such, error models are not simple to implement. Validation of rainfall retrievals with independent data has proven equally difficult due to problems associated with the representativeness of any data source.

Within the Bayesian framework, and *a priori* databases generated from PR observations instead of CRMs, the three error sources not directly dealt with by the Bayesian methodology can be quantified. Errors in the construction of the *a priori* database can be quantified by simply changing assumptions used in the database construction over a reasonable range of values. Because the observations are used to quantify the relative occurrence of various rain realizations, small errors in the database construction are not likely to have significant impacts upon the final result. A major problem encountered when using only CRMs was the completeness and representativeness of the *a priori* databases. With over six years of TRMM radar data representing roughly 10^{10} raining pixels, these issues are no longer a source of uncertainty. Any errors introduced by smaller databases used for computational purposes can be explicitly evaluated.

The second source of error was that introduced by the inversion. Bayes' theorem explicitly accounts for these. It does not, however, account for the

third source of error – regional and seasonal changes in cloud properties. While it seems that these potential biases could be removed by using the appropriate database as determined from the PR data, this is not possible for time periods outside the TRMM era. Conceptually, the simplest method to quantify these errors is to run the retrieval multiple times, changing only the time/space domain for which the database is constructed. Differences between retrievals in this case must be attributed to changes in the rainfall properties that the TRMM radar is able to capture but the radiometer is not. This constitutes a bias error if large space/time domains are considered. A careful analysis using six years of TRMM radar data should be able to quantify the typical magnitude of these errors for use with prior or future radiometer data.

The last source of error is due to any shortcomings in the algorithm formulation. Of particular importance are any changes in parameters that are assumed constant in the forward model or specified incorrectly by the CRMs if these are used. The variational retrieval framework provides a test bed for solving this task to the degree of detail that is resolved by global model cloud/precipitation parameterizations and plane-parallel radiative transfer modeling. Ground-based data can alternatively be used.

5 CONCLUDING REMARKS

The entire algorithm as described does not currently exist. If it did, we could not speak of the “next generation of microwave rainfall algorithms” as implied by the title. Nonetheless, we have attempted to outline a framework, and give specific examples of work currently underway to achieve the goals set forth by new measurement missions and new user demands. There is no doubt that perhaps some of the details are too vague, while some of the illustrative implementations are too detailed and perhaps not optimal. We do not dispute that but instead would encourage new researchers to enhance, refine or simply amend any of the procedures described here for their optimal use. In speaking about a next generation algorithm, we only provided a specific solution to illustrate that improved methodologies are possible over what is currently done without wishing to imply that the specific solution offered here is the only possible solution. Continued impetus provided by the Global Precipitation Mission related research around the world will undoubtedly help to focus and refine the concepts presented here.

6 REFERENCES

- Battaglia, A., C. Kummerow, D.-B. Shin, and C. Williams, 2003: Constraining microwave brightness temperatures by radar bright band observations, *J. Atmos. Oceanic Technol.*, **20**, 856–871.
- Bauer, P., 2001: Including a melting layer in microwave radiative transfer simulation for clouds. *Atmos. Res.*, **57**, 9–30.

- Bauer, P. and N. C. Grody, 1995: The potential of combining SSM/I and SSM/T2 measurements to improve the identification of snowcover and precipitation. *IEEE Trans. Geosci. Remote Sens.*, **33**, 252–261.
- Bauer, P., P. Amayenc, C. D. Kummerow, and E. A. Smith, 2001: Over ocean rainfall retrieval from multi-sensor data of the Tropical Rainfall Measuring Mission. Part II: algorithm implementation. *J. Atmos. Oceanic Technol.*, **18**, 1838–1855.
- Bauer, P., J.-F. Mahfouf, S. Di Michele, F. S. Marzano, and W. S. Olson, 2002: Errors in TMI rainfall estimates over ocean for variational data assimilation. *Quart. J. Roy. Meteor. Soc.*, **128**, 2129–2144.
- Berg, W. and R. Chase, 1992: Determination of mean rainfall from the special sensor microwave/imager (SSM/I) using a mixed lognormal distribution. *J. Atmos. Oceanic Technol.*, **9**, 129–141.
- Chang, A. T. C., L. S. Chiu, C. Kummerow, and J. Meng, 1999: First results of the TRMM microwave imager (TMI) monthly oceanic rain rate: comparison with SSM/I. *Geophys. Res. Lett.*, **26**, 2379–2382.
- Ellison, W. J., S. J. English, K. Lamkaouchi, A. Balana, E. Obligis, G. Deblonde, T. J. Hewison, P. Bauer, G. Kelly, and L. Eymard, 2003: A comparison of new permittivity data for sea water with AMSU, SSM/I and airborne radiometers observations. *J. Geophys. Res.*, **108**, ACL 1-1–1-14.
- Evans, F., F. J. Turk, T. Wong, and G. Stephens, 1995: A Bayesian approach to microwave precipitation retrieval. *J. Appl. Meteor.*, **34**, 260–279.
- Ferraro, R. R. and G. F. Marks, 1995: The development of SSM/I rain rate retrieval algorithms using ground based radar measurements. *J. Atmos. Oceanic Technol.*, **12**, 755–770.
- Grody, N. C., 1991: Classification of snow cover and precipitation using the Special Sensor Microwave/Imager (SSM/I). *J. Geophys. Res.*, **96**, 7423–7435.
- Haddad, Z. S., E. A. Smith, C. Kummerow, T. Iguchi, M. R. Farrar, S. L. Durden, M. Alves, and W. S. Olson, 1997: The TRMM ‘day-1’ radar/radiometer combined rain-profiling algorithm. *J. Meteorol. Soc. Japan*, **75**, 799–808.
- Iguchi, T., T. Kozu, R. Meneghini, J. Awaka, and K. Okamoto, 2000: Rain-profiling algorithm for the TRMM precipitation radar. *J. Appl. Meteor.*, **39**, 2038–2052.
- Kummerow, C., 1993: On the accuracy of the Eddington approximation for radiative transfer in the microwave frequencies. *J. Geophys. Res.*, **98**, 2757–2765.
- Kummerow, C. and L. Giglio, 1994: A passive microwave technique for estimating rainfall and vertical structure information from space, Part I: Algorithm description. *J. Appl. Meteor.*, **33**, 3–18.
- Kummerow, C., W. S. Olson, and L. Giglio, 1996: A simplified scheme for obtaining precipitation and vertical hydrometeor profiles from passive microwave sensors. *IEEE Trans. Geosci. Remote Sens.*, **34**, 1213–1232.
- Kummerow, C., Y. Hong, W. S. Olson, S. Yang, R. F. Adler, J. McCollum, R. Ferraro, G. Petty, D.-B. Shin, and T. T. Wilheit, 2001: The evolution of the Goddard Profiling Algorithm (GPROF) for rainfall estimation from passive microwave sensors. *J. Appl. Meteor.*, **40**, 1801–1820.
- Liebe, H., P. Rosenkranz, and G. Hufford, 1992: Atmospheric 60 GHz oxygen spectrum: New laboratory measurements and line parameters. *J. Quant. Spec. Rad. Trans.*, **48**, 629–643.
- Marzano, F. S. and P. Bauer, 2001: Sensitivity analysis of airborne microwave retrieval of stratiform precipitation to the melting layer parameterization. *IEEE Trans. Geosci. Remote Sens.*, **39**, 75–91.
- Marzano, F. S., A. Mugnai, G. Panegrossi, N. Pierdicca, E. A. Smith, and J. Turk, 1999: Bayesian estimation of precipitating cloud parameters from combined measurements of spaceborne microwave radiometer and radar. *IEEE Trans. Geosci. Remote Sens.*, **37**, 596–613

- Moreau, E., P. Bauer, and F. Chevallier, 2003: Variational retrieval of rain profiles from spaceborne passive microwave radiance observations. *J. Geophys. Res.*, **108**, ACL 11–1 — 11–18.
- Moreau, E., P. Lopez, P. Bauer, A. M. Tompkins, M. Janisková, and F. Chevallier, 2004: Variational retrieval of temperature and humidity profiles using rain-rates versus microwave brightness temperatures. *Quart. J. Roy. Meteor. Soc.*, **130**, 827–852.
- Mugnai, A., E. A. Smith, and G. J. Tripoli, 1993: Foundation of physical-statistical precipitation retrieval from passive microwave satellite measurements. Part II: Emission source and generalized weighting function properties of a time dependent cloud-radiation model. *J. Appl. Meteor.*, **32**, 17–39.
- Olson, W. S., 1989: Physical retrieval of rainfall rates over the ocean by multispectral radiometry: Application to tropical cyclones. *J. Geophys. Res.*, **94**, 2267–2280.
- Olson, W. S., C. D. Kummerow, G. M. Heymsfield, and L. Giglio, 1996: A method for combined passive-active microwave retrievals of cloud and precipitation profiles. *J. Appl. Meteor.*, **38**, 1763–1789.
- Olson, W. S., C. D. Kummerow, Y. Hong, and W.-K. Tao, 1999: Atmospheric latent heating distributions in the tropics derived from satellite passive microwave radiometer measurements. *J. Appl. Meteor.*, **38**, 633–664.
- Olson, W. S., P. Bauer, C. D. Kummerow, Y. Hong, and W.-K. Tao, 2001: A melting-layer model for passive/active microwave remote sensing applications. Part II: Simulations of TRMM observations. *J. Appl. Meteor.*, **40**, 1164–1179.
- Petty, G. W., 1994: Physical retrievals of over-ocean rain rate from multichannel microwave imagery. Part I: Theoretical characteristics of normalized polarization and scattering indices. *Meteor. Atmos. Phys.*, **54**, 79–99.
- Rodgers, C. D., 2000: *Inverse Methods for Atmospheric Sounding: Theory and Practice*. World Scientific Publishing, Co., River Edge, NJ.
- Shin, D.-B. and C. Kummerow, 2003: Parametric rainfall retrieval algorithms for passive microwave radiometers. *J. Appl. Meteor.*, **42**, 1480–1496.
- Smith, E. A., X. Xiang, A. Mugnai, and G. Tripoli, 1994: Design of an inversion-based precipitation profile retrieval algorithm using an explicit cloud model for initial guess microphysics. *Meteor. Atmos. Phys.*, **54**, 53–78.
- Spencer, R. W., D. W. Martin, B. B. Hinton, and J. A. Weinman, 1983: Satellite microwave radiances correlated with radar rain rates over land. *Nature*, **304**, 141–143.
- Viltard, N., C. Burlaud, and C. Kummerow, 2004: Rain retrieval from TMI brightness temperature measurements using a PR-based database. *J. Appl. Meteor. Climatol.*, **45**, 455–466.
- Wentz, F. J., 1997: A well-calibrated ocean algorithm for Special Sensor Microwave/ Imager. *J. Geophys. Res.*, **102** (C4), 8703–8718.
- Wilheit, T. T., A. T. C. Chang, and L. S. Chiu, 1991: Retrieval of monthly rainfall indices from microwave radiometric measurement using probability distribution functions. *J. Atmos. Oceanic Technol.*, **8**, 118–136.